Shaping the dissipative collinear three-wave coupled states in a two-mode medium with a square-law nonlinearity and linear non-optical losses

J. Opt. A: Pure Appl. Opt. **10** (2008) 025001 (10pp) doi:10.1088/1464-4258/10/02/025001

Shaping the dissipative collinear three-wave coupled states in a two-mode medium with a square-law nonlinearity and linear non-optical losses

Alexandre S Shcherbakov[1], **Jewgenij Maximov**[2] **and Sandra E Balderas Mata**[1]

[1] Department of Optics, National Institute for Astrophysics, Optics and Electronics, AP 51 y 216, Puebla 72000, Mexico
[2] Molecular Technology GmbH, Rudower Chaussee 29-31, D-12489 Berlin, Germany

E-mail: alex@inaoep.mx, mtberlin@aol.com (J Maximov) and smata@inaoep.mx

Received 1 August 2007, accepted for publication 17 December 2007
Published 11 January 2008
Online at stacks.iop.org/JOptA/10/025001

Abstract
Dissipative multi-pulse three-wave coupled states, appearing with collinear Bragg light scattering in a two-mode square-law nonlinear medium with linear non-optical losses, are revealed. Both the localization conditions and the spatio-temporal distributions of their optical components are studied theoretically in quasi-stationary and non-stationary regimes. Then, dissipative multi-pulse three-wave coupled states have been observed within the acousto-optical experiments in a calcium molybdate crystalline collinear cell. The obtained experimental results are in rather good agreement with the non-stationary theory developed.

Keywords: dissipative multi-pulse three-wave coupled states, square-law nonlinearity, linear non-optical losses, co-directional collinear Bragg interaction, acousto-optics

(Some figures in this article are in colour only in the electronic version)

1. Introduction

Usually, scattering light in a medium modulated periodically by relatively slow non-optical waves represents the parametric process in a system with square-law nonlinearity. This effect makes possible shaping spatio-temporal multi-wave coupled states and solitons, whose field components can have different physical natures but are coupled with each other [1]. Such a type of multi-pulse three-wave coupled state has been already investigated in lossless two-mode media, waveguides and crystals [2, 3]. Here, a new specific regime is considered, which is related to shaping three-wave Bragg weakly coupled states within the co-directional collinear interaction in a two-mode medium exhibiting the linear losses for a slow non-optical wave. We develop both quasi-stationary and non-stationary analytic models describing the localization processes for multi-pulse three-wave coupled states and present the corresponding computer simulations. Within our quasi-stationary analysis, the mechanism of originating a background, associated with the coupled states under consideration, is investigated, so that these results are taken into account within the non-stationary analysis to examine only background-free regimes of shaping those coupled states. Finally we present and discuss the data obtained due to our experiments with multi-pulse three-wave acousto-optical coupled states in a calcium molybdate ($CaMoO_4$) crystalline collinear cell.

2. General consideration: a three-wave collinear interaction with phase mismatches and linear non-optical losses

A three-wave co-directional collinear interaction with the mismatched wavenumbers in a two-mode medium is described by a set of three nonlinear partial differential equations [4].

Here, we consider the regime of a weak coupling [2, 3], when two light modes are scattered by a relatively slow wave, being non-optical by its nature and exhibiting linear losses, when essentially the effective Bragg scattering of light can be achieved without any observable influence of the scattering process on that non-optical wave, because the number of interacting photons is a few orders less than the number of the scattering quanta injected into a medium. Then, the velocities of light modes can be approximated by the same value c, because usually the length of the crystalline materials does not exceed 10 cm. In this regime, the above-mentioned set of equations falls into an equation for the complex amplitude $U(x,t)$ of a slow wave (v is the velocity of this wave) and a pair of combined equations for the complex amplitudes $C_0(x,t)$ and $C_1(x,t)$ of the incident (pumping) light wave and scattered one, respectively:

$$\frac{\partial U}{\partial x}+\frac{1}{v}\frac{\partial U}{\partial t}=-\alpha U, \tag{1a}$$

$$\frac{\partial C_0}{\partial x}+\frac{1}{c}\frac{\partial C_0}{\partial t}=-q_1 C_1 U^{*}\exp(2\mathrm{i}\eta x), \tag{1b}$$

$$\frac{\partial C_1}{\partial x}+\frac{1}{c}\frac{\partial C_1}{\partial t}=q_0 C_0 U\exp(-2\mathrm{i}\eta x). \tag{1c}$$

Here, the factor α describes the linear losses of the non-optical wave, $q_{0,1}$ are the constants of interaction and 2η is the mismatch of wavenumbers inherent in the interacting waves. Now, we go to the tracking coordinates ($x, \tau = t - x/c$) and assume that the non-optical wave, governed by equation (1*a*) and described by $U = u[x(1-v/c)-v\tau]\exp(-\alpha x)\exp(\mathrm{i}\varphi)$, has the constant phase φ, so that one can convert equations (1*b*) and (1*c*) into equations of the second order

$$\frac{\partial^2 C_{0,1}}{\partial x^2}-\left(\frac{1}{u}\frac{\partial u}{\partial x}-\alpha\pm 2\mathrm{i}\eta\right)\frac{\partial C_{0,1}}{\partial x} + q_0 q_1 u^2\exp(-2\alpha x)C_{0,1}=0. \tag{2}$$

We put $C_{0,1}=a_{0,1}(x,t)\exp[\mathrm{i}\Phi_{0,1}(x,t)]$ and $\gamma_{0,1}=\partial\Phi_{0,1}/\partial x$ and then divide the real and imaginary parts in equation (2) as

$$\frac{\partial^2 a_{0,1}}{\partial x^2}-\left(\frac{1}{u}\frac{\partial u}{\partial x}-\alpha\right)\frac{\partial a_{0,1}}{\partial x} + \left[q_0 q_1 u^2\exp(-2\alpha x)-\gamma_{0,1}^2\pm 2\eta\gamma_{0,1}\right]a_{0,1}=0, \tag{3}$$

$$2\left(\gamma_{0,1}\mp\eta\right)\frac{\partial a_{0,1}}{\partial x}+\left(\frac{\partial\gamma_{0,1}}{\partial x}-\frac{\gamma_{0,1}}{u}\frac{\partial u}{\partial x}+\alpha\gamma_{0,1}\right)a_{0,1}=0. \tag{4}$$

Equation (4) has the following general solutions:

$$\gamma_{0,1}=\pm\eta u a_{0,1}^{-2}\exp(-\alpha x)\int u^{-1}(\partial a_{0,1}^2/\partial x) \times\exp(\alpha x)\,\mathrm{d}x+\Gamma_{0,1}u a_{0,1}^{-2}\exp(-\alpha x), \tag{5}$$

where $\Gamma_{0,1}$ are the integration constants.

3. The quasi-stationary background-free continuous-wave regime; originating the localization condition

At first, we restrict ourselves by the simplest choice of $\Gamma_{0,1}=0$ in equation (5) and study the phenomenon in the continuous-wave regime for both the incident light and the non-optical wave when $u[x(1-v/c)-v\tau]=U_0$ is constant. We analyze equations (3) and (4) with the fixed magnitude of the mismatch η and the practically natural boundary conditions $a_0(x=0,t)=1$, $(\partial a_0/\partial x)(x=0,t)=0$, $a_1(x=0,t)=0$, $(\partial a_1/\partial x)(x=0,t)=q_0U_0$ in a half-infinite medium. In so doing, let us estimate $\gamma_{0,1}$ approximately. Due to the smallness of the factor α, one can suggest that the spatial scale of varying the term $\exp(\alpha x)$ is much larger than the scale of varying the derivative $\partial a_{0,1}^2/\partial x$ in equation (5), so the term $\exp(\alpha x)$ can be factored out from the integral. As a result, we yield $\gamma_{0,1}\approx\pm\eta$ and $-\gamma_{0,1}^2\pm 2\eta\gamma_{0,1}=\eta^2$. Thus, with the notation $q_0q_1U_0^2=\sigma^2$, equation (3) takes the form

$$\frac{\partial^2 a_{0,1}}{\partial x^2}+\alpha\frac{\partial a_{0,1}}{\partial x}+\left[\sigma^2\exp(-2\alpha x)+\eta^2\right]a_{0,1}=0. \tag{6}$$

Recently, equation (6) has been analyzed in the case of $\alpha=0$ and $\eta\neq 0$ [2, 3], while now another possibility will be considered. It should be noted that equation (6) has the following exact analytical solutions in terms of the Bessel functions

$$a_{0,1}=B_{0,1}\exp\left(-\frac{\alpha x}{2}\right)J_{\nu}\left[\exp(-\alpha x)\frac{\sigma}{\alpha}\right] + D_{0,1}\exp\left(-\frac{\alpha x}{2}\right)J_{-\nu}\left[\exp(-\alpha x)\frac{\sigma}{\alpha}\right], \tag{7}$$

where $B_{0,1}$ and $D_{0,1}$, are the integration constants; $\nu=(2\alpha)^{-1}\sqrt{\alpha^2-4\eta^2}$. In the regime of an exact phase synchronism, i.e. with $\eta=0$ and $\alpha\neq 0$, when the indices of Bessel functions in equation (7) are equal to $\pm 1/2$, these solutions can be reduced to

$$a_{0,1}=K_{0,1}\sin\left\{\frac{\sigma}{\alpha}\left[1-\exp(-\alpha x)\right]\right\} + L_{0,1}\cos\left\{\frac{\sigma}{\alpha}\left[1-\exp(-\alpha x)\right]\right\} \tag{8}$$

with

$$B_{0,1}\sqrt{\frac{2\alpha}{\pi\sigma}}=K_{0,1}\cos\left(\frac{\sigma}{\alpha}\right)+L_{0,1}\sin\left(\frac{\sigma}{\alpha}\right)$$

and

$$D_{0,1}\sqrt{\frac{2\alpha}{\pi\sigma}}=K_{0,1}\sin\left(\frac{\sigma}{\alpha}\right)+L_{0,1}\cos\left(\frac{\sigma}{\alpha}\right).$$

Applying the above-mentioned natural boundary conditions to equation (8), one can obtain

$$|C_0(x)|^2=\cos^2\left\{\frac{\sigma}{\alpha}\left[1-\exp(-\alpha x)\right]\right\}, \tag{9a}$$

$$|C_1(x)|^2=\frac{q_0}{q_1}\sin^2\left\{\frac{\sigma}{\alpha}\left[1-\exp(-\alpha x)\right]\right\}. \tag{9b}$$

It is seen from equations (9) that the contribution of the linear losses from the non-optical wave exhibits itself like some spatial scaling in light scattering, while the efficiency of light scattering can nevertheless achieve 100% with $\eta=0$ and $\alpha\neq 0$.

However, the form of general solution to equation (6), represented by equation (7), is not quite convenient in practically important cases of large phase mismatches, when $\eta>\alpha$. To construct the other form of the solution we use the

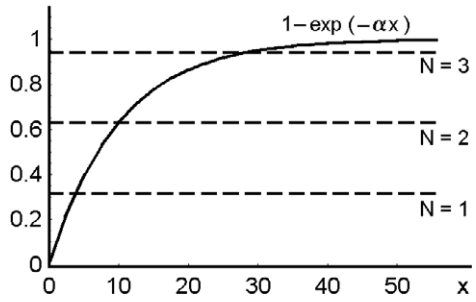

Figure 1. Restricting the number N of pulses inherent in a three-wave coupled state in the case of $\eta = 0$ and $\alpha \neq 0$; for an example of $\alpha = 0.1$ and $\sigma = 1$, one can find that $N \leqslant 3$.

conservation law $q_0 a_0^2 + q_1 a_1^2 = q_0 - \text{const}$, resulting from equations (1). Combining equation (6) for a_0 and a_1, one can obtain a pair of the following equations:

$$\frac{\partial (a_{0,1}^2)}{\partial x} = 2\sqrt{a_{0,1}^2 (q_{0,1}^{-1} q_0 - a_{0,1}^2)[\sigma^2 \exp(-2\alpha x) + \eta^2]}, \quad (10)$$

whose solutions with arbitrary integration constants $\theta_{0,1}$ are given by

$$a_{0,1}^2 = q_{0,1}^{-1} q_0 \sin^2 \left[\theta_{0,1} + G\,(x)\right], \quad (11a)$$

$$G\,(x) = \int \sqrt{\sigma^2 \exp(-2\alpha x) + \eta^2}\, \mathrm{d}x. \quad (11b)$$

Using the above-noted boundary conditions, we arrive at

$$\theta_0 = \arcsin\left[\sigma^{-1}\sqrt{\sigma^2 + \eta^2}\right] - G(0), \quad (12a)$$

$$\theta_1 = -G(0), \quad (12b)$$

$$G(x) = \frac{1}{\alpha}\left[-\sqrt{\eta^2 + \sigma^2 \exp(-2\alpha x)} + \eta \ln\left\{\frac{2\alpha}{\eta^2}\left[\eta \exp(\alpha x) + \sqrt{\sigma^2 + \eta^2 \exp(2\alpha x)}\right]\right\}\right] \quad (12c)$$

$$G\,(0) = \frac{1}{\alpha}\left(-\sqrt{\eta^2 + \sigma^2} + \eta \ln\left\{2\alpha\eta^{-2}\left[\eta + \sqrt{\sigma^2 + \eta^2}\right]\right\}\right) \quad (12d)$$

so that the stationary intensities of the pumping and scattered light waves can be expressed as

$$|C_0(x)|^2 = \frac{\eta^2}{\sigma^2 + \eta^2} + \frac{\sigma^2}{\sigma^2 + \eta^2}\cos^2[G(x) - G(0)], \quad (13a)$$

$$|C_1(x)|^2 = \frac{q_0}{q_1}\frac{\sigma^2}{\sigma^2 + \eta^2}\sin^2[G(x) - G(0)]. \quad (13b)$$

These solutions include contributions of two types. The first summand in the intensity $|C_0|^2$ represents a background determined by the mismatch η; the second one gives the oscillations imposed on that background. The scattered light wave contains only oscillations, so that one can write the localization condition

$$G(x) - G(0) = \pi N, \quad (14)$$

where $(N = 1, 2, \ldots)$. Of course, when $\eta = 0$, we yield $G(x) = -\alpha^{-1}\sigma \exp(-\alpha x)$, $\theta_0 = \alpha^{-1}\sigma + (\pi/2)$ and $\theta_1 = \alpha^{-1}\sigma$, so that equations (13) take the form of equations (9). The fact of the existence of this localization condition means the dissipative collinear three-wave coupled states appearing in a two-mode medium with square-law nonlinearity and linear losses for a slow non-optical wave; and they can include more than one pulse when $N > 1$.

Additionally, it should be noted that a pair of the obtained solutions for the intensities $I_{0,1} = |C_{0,1}|^2$ described by equations (13) satisfy the following differential equations:

$$\left(\frac{\mathrm{d}G}{\mathrm{d}x}\right)^{-2}\frac{\partial^2 I_0}{\partial x^2} + \alpha\left(\frac{\mathrm{d}G}{\mathrm{d}x}\right)^{-4}\left[\left(\frac{\mathrm{d}G}{\mathrm{d}x}\right)^2 - \eta^2\right]\frac{\partial I_0}{\partial x} + 4I_0 = 2\left(\frac{\sigma^2 + 2\eta^2}{\sigma^2 + \eta^2}\right), \quad (15)$$

$$\left(\frac{\mathrm{d}G}{\mathrm{d}x}\right)^{-2}\frac{\partial^2 I_1}{\partial x^2} + \alpha\left(\frac{\mathrm{d}G}{\mathrm{d}x}\right)^{-4}\left[\left(\frac{\mathrm{d}G}{\mathrm{d}x}\right)^2 - \eta^2\right]\frac{\partial I_1}{\partial x} + 4I_1 = \frac{2q_0}{q_1}\left(\frac{\sigma^2}{\sigma^2 + \eta^2}\right) \quad (16)$$

with the previously noted boundary conditions $I_0(x = 0) = 1$, $I_1(x = 0) = 0$ and $(\partial I_0/\partial x)(x = 0) = (\partial I_1/\partial x)(x = 0) = 0$. The relation $q_0(\partial I_0/\partial x) = -q_1(\partial I_1/\partial x)$ takes place, of course, within the process under consideration.

Then, the number of bright or dark pulses N in the corresponding component of the coupled state is conditioned by both the frequency mismatch η as well as by the losses α. Let us consider a few particular cases. In the first lossless case of $\alpha = 0$ and $\eta \neq 0$, one can obtain from equation (14)

$$\eta^2 = \pi^2 N^2 x_{\mathrm{C}}^{-2} - \sigma^2, \quad (17a)$$

$$G(x) - G(0) = \frac{\pi N x}{x_{\mathrm{C}}}, \quad (17b)$$

where x_{C} is the spatial length of localization. One can substitute this formula into equation (13*b*) and yield the dependence of the scattered light intensity I_1 on the number N of pulses in a coupled state in the form

$$I_1^{(N)}(x, \alpha = 0) = \frac{q_0}{q_1}\frac{\sigma^2 x_{\mathrm{C}}^2}{\pi^2 N^2}\sin^2\left(\frac{\pi N x}{x_{\mathrm{C}}}\right). \quad (18)$$

It is seen from equation (18) that, as the number N grows, the intensity I_1 of the scattered light component in a three-wave coupled state decreases as N^2, because the mismatch increases following equation (17). At the same time, the spatial width $x_{\mathrm{C}}/(\pi N)$ of each partial optical pulse inherent in this coupled state narrows as N^{-1}.

By contrast, in the second particular case of an exact phase synchronism when $\eta = 0$ and $\alpha \neq 0$, equation (14) leads to the formula $\alpha^{-1}\sigma[1 - \exp(-\alpha x)] = \pi N$. Because the left-hand side of this formula is limited, one can find that $N \leqslant \sigma/(\alpha\pi)$, i.e. the whole number N comes to be restricted. For example, when $\alpha = 0.1$ and $\sigma = 1$, we yield $N \leqslant 3$, see figure 1.

In the general case, when $\eta \neq 0$ and $\alpha \neq 0$, a transcendental equation relative to both η and α appears from equations (14) and (12). That is why this case requires numerical simulations presented in figure 2.

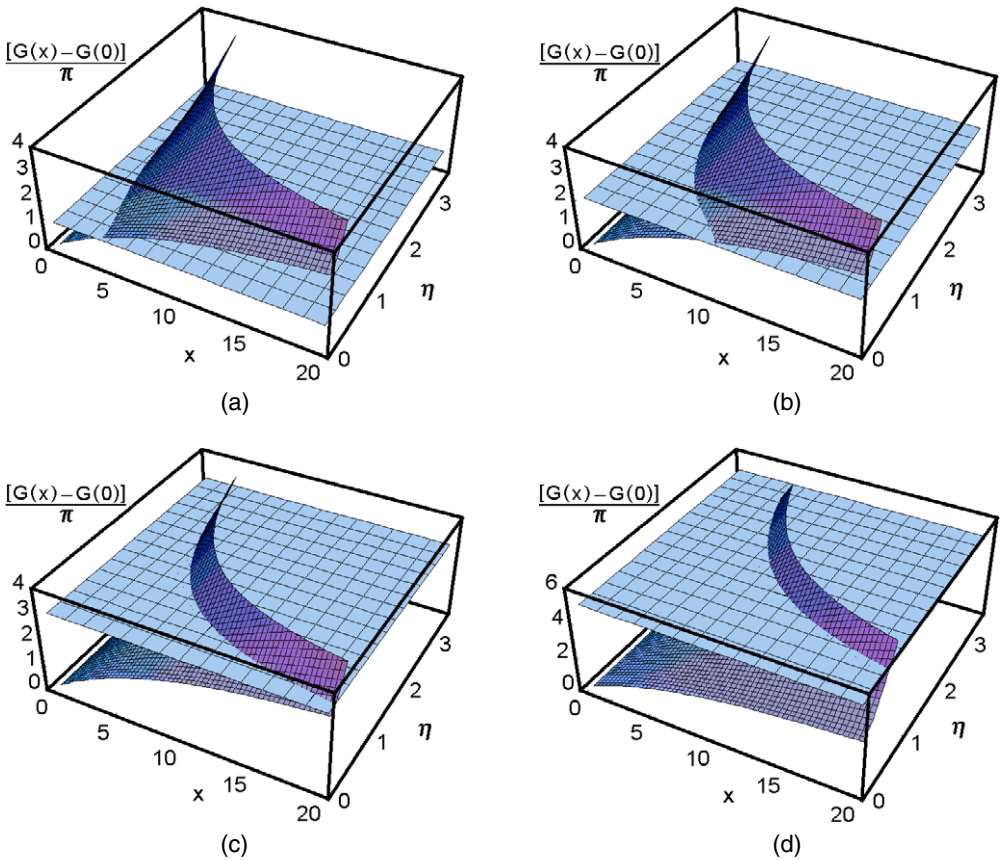

Figure 2. The possibility of shaping multi-pulse coupled states in the case of $\eta \neq 0$ and $\alpha \neq 0$; for an example of $\alpha = 0.1$ and $\sigma = 1$, one can realize: (a) $N = 1$, (b) $N = 2$, (c) $N = 3$ and (d) $N = 5$.

Nevertheless, in the practically important case of low losses for the non-optical wave, one can develop an approximate approach illustrating the effect of losses. In this case, one can put in the first approximation that $\exp(-2\alpha x) \approx 1 - 2\alpha x$ and integrate equation (11*b*) as

$$G(x, \alpha \to 0) = \sqrt{\sigma^2(1 - 2\alpha x) + \eta^2} \times \left(\frac{2x}{3} - \frac{\sigma^2 + \eta^2}{3\alpha\sigma^2}\right), \tag{19a}$$

$$G(x = 0, \alpha \to 0) = -\frac{(\sigma^2 + \eta^2)^{3/2}}{3\alpha\sigma^2}. \tag{19b}$$

Equations (19) lead to

$$G(x, \alpha \to 0) - G(x = 0, \alpha \to 0) = \frac{(\sigma^2 + \eta^2)^{3/2} - (\sigma^2 + \eta^2 - 2\alpha x)^{3/2}}{3\alpha\sigma^2}. \tag{20}$$

In the first approximation with respect to the factor α, equation (12) takes the form

$$G(x, \alpha \to 0) - G(x = 0, \alpha \to 0) = x\sqrt{\sigma^2 + \eta^2} - \frac{\alpha x^2\sigma^2}{2\sqrt{\sigma^2 + \eta^2}}. \tag{21}$$

Consequently, using equations (21) and (17*b*), one can rewrite the localization condition as

$$G(x = x_C, \alpha \to 0) - G(x = 0, \alpha \to 0) = x_C\sqrt{\sigma^2 + \eta^2} - \frac{\alpha x_C^2\sigma^2}{2\sqrt{\sigma^2 + \eta^2}} = \pi N. \tag{22}$$

Considering equation (22) as the algebraic quadratic equation relative to $\sqrt{\sigma^2 + \eta^2}$, one can find

$$\sqrt{\sigma^2 + \eta^2} = \frac{\pi N}{x_C} + \frac{\alpha x_C^2\sigma^2}{2\pi N}. \tag{23}$$

Substituting this formula into equation (13*b*), one can estimate the factor

$$\frac{\sigma^2}{\sigma^2 + \eta^2} \approx \frac{x_C^2\sigma^2}{\pi^2 N^2 + \alpha x_C^3\sigma^2}, \tag{24}$$

so that equation (18) takes the following approximate form:

$$I_1^{(N)}(x, \alpha \neq 0) = \frac{q_0}{q_1}\frac{x_C^2\sigma^2}{\pi^2 N^2 + \alpha x_C^3\sigma^2}\sin^2\left(\frac{\pi N x}{x_C}\right). \tag{25}$$

It is seen from equation (25) again that, as the number N of pulses in a coupled state grows, the intensity $I_1^{(N)}$ of the scattered light decreases, but now even a little bit faster than as N^2, as it was in equation (18), due to the contribution of losses connected with the presence of the term including a small factor α in the denominator of equation (25).

4. The quasi-stationary continuous-wave regime with $\Gamma \neq 0$; a background appearing

Now, we take the case of $\Gamma \neq 0$ and consider this phenomenon again in the continuous-wave regime for the incident light

and the non-optical wave with previously formulated boundary conditions in a half-infinite medium. Estimating $\gamma_{0,1}$ from equation (5) approximately as above, one can write now

$$\gamma_{0,1} \approx \pm\eta + \Gamma_{0,1} U_0 a_{0,1}^{-2} \exp(-\alpha x), \tag{26a}$$

$$-\gamma_{0,1}^2 \pm 2\eta\gamma_{0,1} = \eta^2 + \Gamma_{0,1}^2 U_0^2 a_{0,1}^{-4} \exp(-2\alpha x). \tag{26b}$$

As a result, equations (3) take the following form:

$$\frac{\partial^2 a_{0,1}}{\partial x^2} + \alpha \frac{\partial a_{0,1}}{\partial x} + \left[\sigma^2 \exp(-2\alpha x) + \eta^2\right] a_{0,1} = \Gamma_{0,1}^2 U_0^2 a_{0,1}^{-4} \exp(-2\alpha x). \tag{27}$$

It is seen that equation (27) is the same for the amplitudes a_0 and a_1, so that the indices of waves can be omitted in further analysis. Let us introduce a new independent variable $\zeta = \alpha^{-1}[1 - \exp(-\alpha x)]$ and convert equation (27) into the Ermakov equation [5, 6]

$$\frac{\partial^2 a}{\partial \zeta^2} + \left[\sigma^2 + \eta^2 (1 - \alpha\zeta)^{-2}\right] a = \Gamma^2 U_0^2 a^{-3}. \tag{28}$$

The general solution to equation (28) has the form [6]

$$a^2(\zeta) = M_1^{-1} W^2(\zeta) \left[\Gamma^2 U_0^2 + \left(M_2 + M_1 \int W^{-2}(\zeta)\, \mathrm{d}\zeta\right)^2\right], \tag{29}$$

where $M_{1,2}$ are the integration constants and $W(\zeta)$ is a non-trivial solution to the reduced, i.e. linearized in fact, form of equation (28), namely, to

$$\frac{\partial^2 a_r}{\partial \zeta^2} + \left[\sigma^2 + \eta^2 (1 - \alpha\zeta)^{-2}\right] a_r = 0. \tag{30}$$

Equation (30) has an exact solution in terms of the Bessel functions

$$a_r(\zeta) = Z_1 \sqrt{1 - \alpha\zeta}\, J_{-\nu}\left[(1 - \alpha\zeta)\frac{\sigma}{\alpha}\right] + Z_2 \sqrt{1 - \alpha\zeta}\, J_{\nu}\left[(1 - \alpha\zeta)\frac{\sigma}{\alpha}\right], \quad \nu = \frac{\sqrt{\alpha^2 - 4\eta^2}}{2\alpha}, \tag{31}$$

with the integration constants $Z_{1,2}$. This solution shows that one can take, for example, the following non-trivial functions $W(\zeta)$:

$$W_1(\zeta) = \sqrt{1 - \alpha\zeta}\, J_{-\nu}\left[(1 - \alpha\zeta)\frac{\sigma}{\alpha}\right], \tag{32a}$$

$$W_2(\zeta) = \sqrt{1 - \alpha\zeta}\, J_{\nu}\left[(1 - \alpha\zeta)\frac{\sigma}{\alpha}\right]. \tag{32b}$$

Unfortunately, in the general case, the integral term in equation (29) cannot be calculated in the closed form with $W = W_{1,2}(\zeta)$, while it can be found in a lot of concrete cases. That is why to illustrate the contributions of the factors $\Gamma_{0,1} \neq 0$ one can analyze the rather simple particular case of the absence of mismatches, i.e. when $\eta \equiv 0$. In so doing, rather then operate over equations (32), it would be definitely simpler to take the Ermakov equation appearing from equation (28) with $\eta = 0$, namely

$$\frac{\partial^2 a}{\partial \zeta^2} + \sigma^2 a = \Gamma^2 U_0^2 a^{-3}. \tag{33}$$

The corresponding non-trivial solutions to the linearized form of equation (33) can be found from the formula

$$a_r(\zeta, \eta = 0) = Y_1 \sin(\sigma\zeta) + Y_2 \cos(\sigma\zeta), \tag{34}$$

where $Y_{1,2}$ are the integration constants. For example, one can choose

$$W_1(\zeta, \eta = 0) = \sin(\sigma\zeta), \tag{35a}$$

$$W_2(\zeta, \eta = 0) = \cos(\sigma\zeta). \tag{35b}$$

Now, we introduce a new dependent variable $b(\zeta) = a^2(\zeta) \geqslant 0$ and convert equation (33) into another equivalent form:

$$\frac{b}{2}\frac{\partial^2 b}{\partial \zeta^2} - \frac{1}{4}\left(\frac{\partial b}{\partial \zeta}\right)^2 + \sigma^2 b^2 = \Gamma^2 U_0^2. \tag{36}$$

Equation (36) shows that, as far as $\Gamma \neq 0$, an arbitrary solution $b(\zeta) \geqslant 0$ will include a background, because equation (36) with $\Gamma \neq 0$ cannot be satisfied at the points ζ_0 wherein $b(\zeta_0) = 0$ and $(\mathrm{d}b/\mathrm{d}\zeta)(\zeta_0) = 0$ simultaneously. Then, substituting equations (35) into equation (29) and using the new variable $b(\zeta)$, one can obtain two rather different solutions to equation (33) as well as to equation (36):

$$b_1(\zeta, \eta = 0) = G_1^{-1} \sin^2(\sigma\zeta) \times \left\{\Gamma^2 U_0^2 + \left[H_1 - \sigma^{-1} G_1 \cot(\sigma\zeta)\right]^2\right\}, \tag{37}$$

$$b_2(\zeta, \eta = 0) = G_2^{-1} \cos^2(\sigma\zeta) \times \left\{\Gamma^2 U_0^2 + \left[H_2 + \sigma^{-1} G_2 \tan(\sigma\zeta)\right]^2\right\}, \tag{38}$$

where $G_{1,2}$ and $H_{1,2}$ are the integration constants. In terms of the coordinate x, equations (37) and (38) take the following forms:

$$b_1(x, \eta = 0) = G_1^{-1} \sin^2\left\{\frac{\sigma}{\alpha}\left[1 - \exp(-\alpha x)\right]\right\}\left[\Gamma^2 U_0^2 + \left(H_1 - \frac{G_1}{\sigma}\cot\left\{\frac{\sigma}{\alpha}\left[1 - \exp(-\alpha x)\right]\right\}\right)^2\right], \tag{39}$$

$$b_2(x, \eta = 0) = G_2^{-1} \cos^2\left\{\frac{\sigma}{\alpha}\left[1 - \exp(-\alpha x)\right]\right\}\left[\Gamma^2 U_0^2 + \left(H_2 + \frac{G_2}{\sigma}\tan\left\{\frac{\sigma}{\alpha}\left[1 - \exp(-\alpha x)\right]\right\}\right)^2\right]. \tag{40}$$

Using equations (39) and (40), one can find the boundary values at $x = 0$ as $b_1(x = 0, \eta = 0) = G_1\sigma^{-2}$ and $b_2(x = 0, \eta = 0) = G_2^{-1}(\Gamma^2 U_0^2 + H_2^2)$. Typical illustrative plots for the solution $b_2(x, \eta = 0)$ with various constants are presented in figure 3 by solid lines. Together with this, one can estimate the frequency distribution along a wave using the above-obtained equation (26*a*) $\gamma_{0,1} \approx \pm\eta + \Gamma_{0,1} U_0 a_{0,1}^{-2} \exp(-\alpha x)$. On the one hand, such an estimation will be non-trivial only when $\Gamma \neq 0$, while on the other hand, the regime of an exact phase synchronism with $\eta = 0$ is under consideration at the moment. Consequently, the expression for the frequency γ has to be written as $\gamma \approx \Gamma U_0 b_2^{-1} \exp(-\alpha x)$. The corresponding plot is shown by a dotted line only in figure 3(a) related to the case of $\Gamma \neq 0$, whereas the frequency γ is equal to zero for the cases depicted in figures 3(b) and (c).

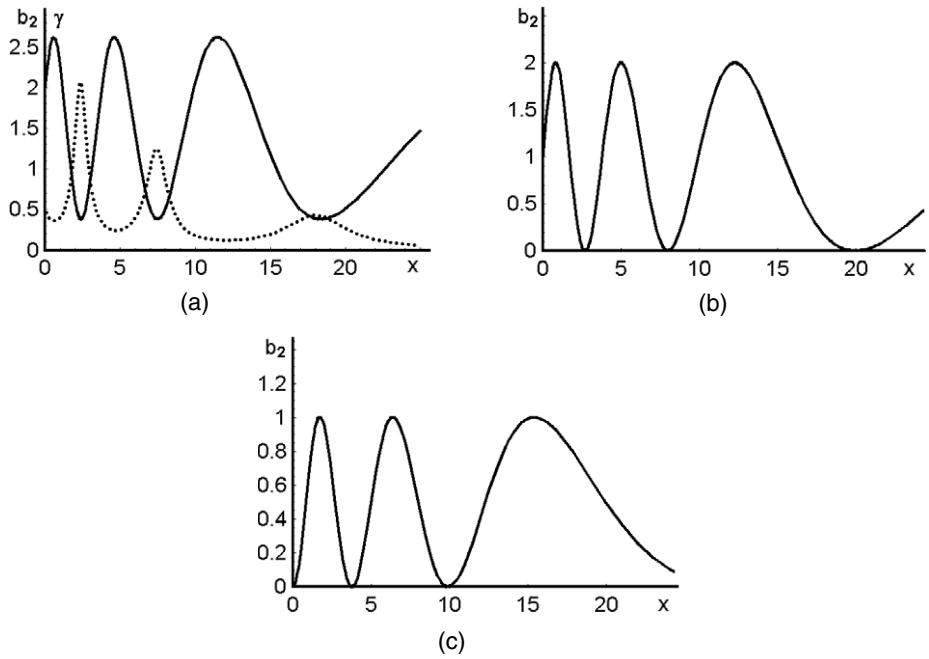

Figure 3. Plots for the solution $b_2(x, \eta = 0)$ with $\sigma = 1$, $\alpha = 0.1$ and $G_2 = 1$: (a) $H_2 = 1$, $\Gamma^2 U_0^2 = 1$, (solid line is for b_2, dotted line is for the frequency γ); (b) $H_2 = 1$, $\Gamma^2 U_0^2 = 0$; (c) $H_2 = 0$, $\Gamma^2 U_0^2 = 0$.

5. Non-stationary regime of the pulsed non-optical wave and localizing multi-pulse three-wave weakly coupled states

Now, we focus our attention on the process of localizing multi-pulse three-wave coupled states when the incident light is continuous-wave in behavior, but two facets of a medium at $x = 0$ and L bound the area of interaction and the pulsed non-optical wave is excited in a medium. We assume that the spatial length x_0 of the non-optical pulse is much shorter than the length L ($T_0 = x_0/v \ll T = L/v$) and that the non-optical pulse has a rectangular shape, i.e. $u(x, t) = U_0\{\theta[x(1 - v/c) - v\tau] - \theta[(x - x_0)(1 - v/c) - v\tau]\}$ with the amplitude U_0. Due to $v \ll c$, we may put that $\partial u/\partial x \approx 0$ in equations (3) and (4) everywhere, excluding the points $x \in \{0, x_0\}$. These practically reasonable suppositions lead to the appearance of three stages in the localization process. In the first stage, the localizing rectangular non-optical pulse is incoming through the input facet $x = 0$ of a medium. Then, in the second stage, this localizing non-optical pulse is passed along a medium and fills the linear losses. Finally, the loss-perturbed non-optical pulse issues through the output facet $x = L$ of a medium. Such a process can be described analytically by the following equations:

$$|C_0(x, \tau)|^2 = \frac{\eta^2}{\sigma^2 + \eta^2} + \frac{\sigma^2}{\sigma^2 + \eta^2} \cos^2[\Phi(x, \tau)], \quad (41a)$$

$$|C_1(x, \tau)|^2 = \frac{q_0}{q_1} \frac{\sigma^2}{\sigma^2 + \eta^2} \sin^2[\Phi(x, \tau)], \quad (41b)$$

where the argument of trigonometric functions in equations (41) for each of the above-mentioned stages can be described as

$$\Phi(x, \tau) = \begin{cases} G(x) - G(0), & 0 \leqslant \tau \leqslant T; \\ G(x) - G(x - x_0), & \\ \qquad T \leqslant \tau \leqslant x(c - v)/(cv); & \\ G(L) - G(x - x_0), & \\ \qquad x(c-v)/(cv) \leqslant \tau \leqslant T + x(c-v)/(cv); & \\ 0, \qquad \tau < 0 \text{ or } \tau > T + x(c - v)/(cv). & \end{cases} \quad (42)$$

The first summand in equation (41*a*) exhibits a background of the light wave $|C_0|^2$, whose level is determined by the mismatch η; the second one represents the oscillating portion of the solution, i.e. the localized part of the incident light imposed on a background. The light wave $|C_1|^2$ contains the only oscillating portion of the light field that gives the localization condition $G(x_C) - G(0) = \pi N$, being perfectly analogous to equation (14); here, x_C is the spatial size of localization area with $v \ll c$ and $N = 0, 1, 2, \ldots$. Figure 4 illustrates the numerical simulations of equations (41*b*) and (42) or the wave $|C_1|^2$. The corresponding numerical plots for the wave $|C_0|^2$ can be easily created using the above-mentioned conservation law $q_0 a_0^2 + q_1 a_1^2 = q_0 -$ const.

From the viewpoint of further experimental verification, these plots can be interpreted rather simply. Depending on the practically fixed length L of a two-mode medium sample, one can consider a cross section of each of these plots with the selected plane $L =$ const to obtain the corresponding one-dimensional theoretical curve in time domain related to the chosen value of a mismatch. Thus, taking alone perfectly localized states presented here in figure 4(b) for $N = 1$ and in figure 4(d) for $N = 2$, one can see that it is possible to

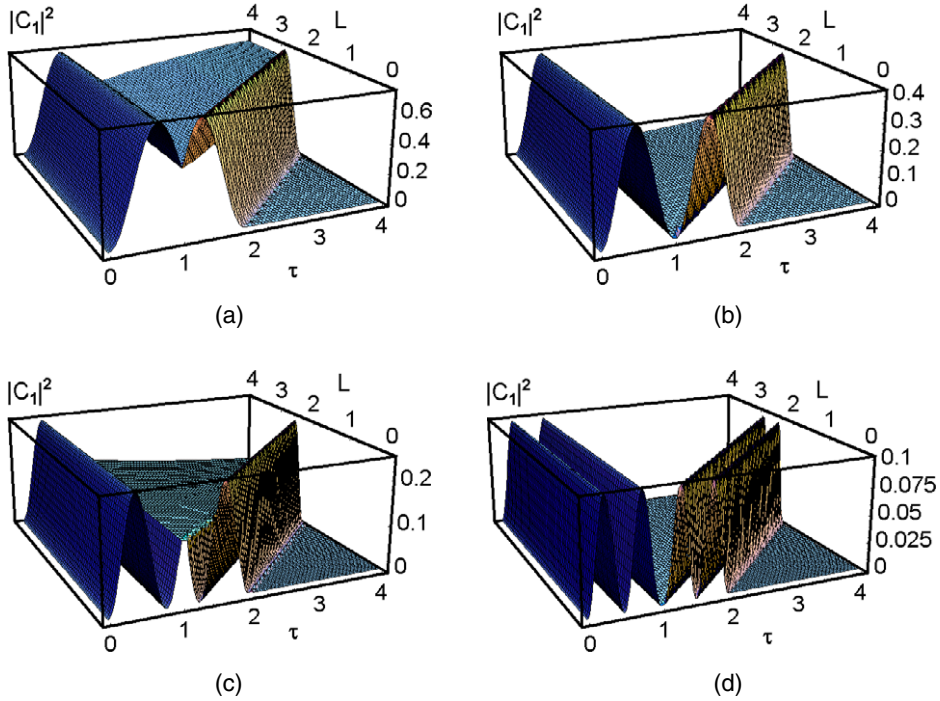

Figure 4. Intensity of the scattered light component inherent in a three-wave coupled state versus the time τ and the length L with $\sigma = 2$, $\alpha = 0.05$. Four various regimes of reshaping have been simulated: (a) $\eta = 1.5$, the beginning regime of shaping a one-pulse coupled state; (b) $\eta = 2.4$, a one-pulse coupled state; (c) $\eta = 3.5$, an intermediate regime; and (d) $\eta = 6.0$, a two-pulse coupled state.

observe the localized field associated with the scattered light component $|C_1|^2$ for two times, namely, when the localizing non-optical pulse is incoming or issuing through one of the facets of a medium creating or destroying, respectively, the corresponding multi-pulse three-wave coupled state.

6. Preliminary estimations

Now let us consider a few practically useful estimations related to experimental observation of the dissipative collinear three-wave coupled states in a two-mode medium with a square-law nonlinearity and linear non-optical losses. In so doing, one can select such a physical phenomenon as the collinear acousto-optical interaction with linear acoustic losses in a two-mode crystalline cell made of a calcium molybdate ($CaMoO_4$) single crystal. In this particular case, one can observe only the anomalous process of light scattering [7] when the states of polarization for the incident and scattered light beams are orthogonal to each other, so that the parameters $q_{0,1}$ are described [8] by

$$q_{0,1} = \frac{\left|\vec{k}_{0,1}\right|}{4n_{0,1}^2}(\vec{e}_0 \Delta\varepsilon \vec{e}_1). \tag{43}$$

Here, $n_{0,1}$ are the refractive indices for the interacting light waves, $|\vec{k}_{0,1}| = 2\pi n_{0,1}/\lambda$, λ is the light wavelength in a vacuum and the last term in brackets, describing the efficiency of interaction, is subject to finding. This term includes the eigen-orts $\vec{e}_{0,1}$ of polarizations for the incident and scattered light beams as well as the tensor $\Delta\varepsilon$ of perturbations of the dielectric permittivity under action of the acoustic wave in a medium. To estimate the efficiency of collinear acousto-optical interaction in a calcium molybdate cell, i.e. to find the contribution of brackets to equation (43), we consider the geometry of interaction including the shear acoustic wave with the wave normal ort $\vec{m}$ is passing along the [100] axis, while its vector $\vec{u}$ of the transversal elastic displacements is oriented along the [001] axis in that crystalline material, i.e. $\vec{m} = [1, 0, 0]$ and $\vec{u} = [0, 0, 1]$. Consequently, one can write the deformation tensor γ and the unperturbed dielectric permittivity tensor ε in the main crystallographic axes as

$$\gamma = \frac{\gamma_0}{2}(\vec{u}\cdot\vec{m} + \vec{m}\cdot\vec{u}) = \frac{\gamma_0}{2}\begin{pmatrix} 0 & 0 & 1 \\ 0 & 0 & 0 \\ 1 & 0 & 0 \end{pmatrix}, \tag{44a}$$

$$\varepsilon = \begin{pmatrix} \varepsilon_0 & 0 & 0 \\ 0 & \varepsilon_0 & 0 \\ 0 & 0 & \varepsilon_e \end{pmatrix}. \tag{44b}$$

Here, γ_0 is the amplitude of the shear deformation, while $\varepsilon_0 = n_0^2$ and $\varepsilon_e = n_e^2$ are the eigenvalues of the unperturbed dielectric permittivity tensor ε. Now, the tensor γ of the second rank with the components γ_{kl} $(k, l = 1, 2, 3)$ can be converted into a six-dimensional vector $\bar{\gamma} = \gamma_0(0, 0, 0, 0, 1, 0)$ with the components $\bar{\gamma}_\mu$ $(\mu = 1, \ldots, 6)$ using the standard procedure [9], which includes re-notating $\bar{\gamma}_\mu = \gamma_{kk}$ $(\mu = 1, 2, 3)$ and $\bar{\gamma}_\mu = 2\gamma_{kl}$ $(k \neq l, \mu = 4, 5, 6)$. If now one will use the same procedure [9] and take the photo-elastic tensor p of the fourth rank for a calcium molybdate single crystal in the form of a 6 x 6 matrix $\hat{p}$, it will be possible first to construct and to calculate the product $\hat{p}\bar{\gamma} = \gamma_0(0, 0, 0, p_{45}, p_{44}, 0)$, and then to convert

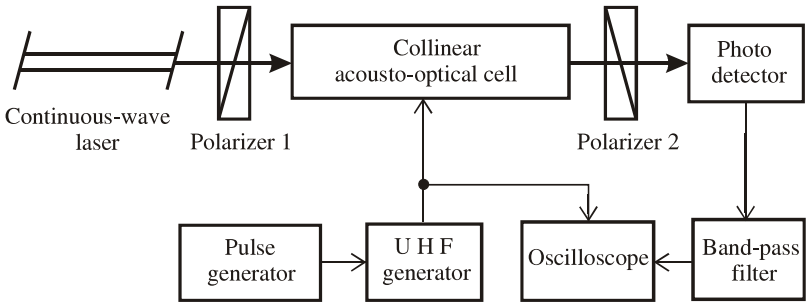

Figure 5. Schematic arrangement of the experimental set-up.

the result back to the form of a standard tensor $(p\gamma)$ of the second rank.

The next step of our analysis is connected with finding the dielectric permittivity perturbation tensor $\Delta\varepsilon$, whose components can be written as $\Delta\varepsilon_{ij} = \varepsilon_{im}\varepsilon_{nj}p_{mnkl}\gamma_{kl}$ [8]. The result of similar calculations has the form

$$\Delta\varepsilon = \gamma_0\varepsilon_0\varepsilon_e \begin{pmatrix} 0 & 0 & p_{44} \\ 0 & 0 & p_{45} \\ p_{44} & p_{45} & 0 \end{pmatrix}. \tag{45}$$

Now, we take into account the orts $\vec{e}_{0,1}$ of polarization for the incident and scattered light waves. When the wave vectors of these light waves are collinear to the wave normal ort $\vec{m}$ for the acoustic wave and, of course, to the [100] axis in the calcium molybdate crystal, the eigen-orts $\vec{e}_{0,1}$ of light polarizations should be oriented, as directly follows from equation (44*b*), along the [0, 1, 0] and [0, 0, 1] axes, so that one can take, for example, $\vec{e}_0 = [0, 1, 0]$ and $\vec{e}_1 = [0, 0, 1]$ with $n_0 = n_o$ and $n_1 = n_e$. As a result, one can obtain the contribution of brackets to equation (43) as

$$\vec{\tilde{e}}_0\Delta\varepsilon\vec{e}_1 = \vec{\tilde{e}}_1\Delta\varepsilon\vec{e}_0 = \gamma_0\varepsilon_0\varepsilon_e p_{45}. \tag{46}$$

In so doing, one can find that $q_{0,1} = \pi(2\lambda)^{-1}n_{e,o}\gamma_0 n_{o,e}^2 p_{45}$. One can see now that the difference between q_0 and q_1 is rather small, because $q_0/q_1 = n_e/n_o$. Then, because the amplitude of deformation can be explained as $\gamma_0 = \sqrt{2P/(\rho V^3)}$, where P is the acoustic power density, one can finally obtain

$$q_0 = \frac{\pi}{\lambda}\sqrt{\frac{P}{2}\left(\frac{n_e^2 n_o^4 p_{45}^2}{\rho V^3}\right)}, \tag{47a}$$

$$q_1 = \frac{\pi}{\lambda}\sqrt{\frac{P}{2}\left(\frac{n_o^2 n_e^4 p_{45}^2}{\rho V^3}\right)}. \tag{47b}$$

It should be noted that the factors taken in brackets in equations (47) represent the acousto-optical figures of merit M_2 peculiar to estimating the efficiency of crystalline materials in acousto-optics [10].

At this step, we are ready to perform a few numerical estimations. Let us start from estimating the acousto-optical figure of merit M_2 peculiar to the geometry of collinear interaction under consideration at a wavelength λ of 0.532 μm in a calcium molybdate cell. Taking the material density $\rho = 4.34$ g cm^{-3}, acoustic velocity $V = 2.95 \times 10^5$ cm s^{-1}, $p_{45} = 0.06$, $n_e = 2.0239$ and $n_o = 2.0116$ at the chosen light wavelength [11], one can calculate $M_2 \approx 2.07\times10^{-18}$ cm^3 g^{-1} in a quite acceptable approximation of $q_0 \approx q_1$, i.e. with an accuracy of about 1%.

Then, one can restrict oneself by a maximal level $P = 0.5$ W mm^{-2} of the acoustic power density and estimate the factor $\sigma = U_0\sqrt{q_0 q_1}$. This level of the power density P is conditioned by the absolute acoustic power magnitude of about 2 W and the acoustic beam cross section of about 4 mm^2 in just a collinear acousto-optical cell. Consequently, one can find that $\sigma \approx 2$ cm^{-1}.

Together with this, one can estimate the potential contributions of both the angular-frequency mismatch and the acoustic losses. Maximal value of the mismatch parameter $\eta = \pi\Delta f/V$ for a frequency detuning Δf of 0.6 MHz is equal to about 6.4 cm^{-1}. The coefficient of linear attenuation for the chosen shear acoustic wave passing along the [100] axis is $\Gamma = 60$ dB cm^{-1} GHz^{-2} in a calcium molybdate single crystal [11]. The factor α of acoustic losses, measured in cm^{-1}, can be expressed via the standard relation as α (cm^{-1}) $=$ 0.23Γ (dB cm^{-1} GHz^{-2}) f^2 (GHz). Thus, at a carrier frequency f_0 of about 60 MHz related to the above-mentioned light wavelength of 0.532 μm, being peculiar to the collinear acousto-optical interaction in calcium molybdate, one can estimate the factor of acoustic losses as $\alpha = 0.05$ cm^{-1} in the case under consideration. Additionally, it should be noted that our theoretical numerical data, presented in the previous section 5, were normalized in such a way that those dimensionless values are in coincidence with practical numerical estimations presented in this section. This fact provides easy comparison of the theoretical and experimental data with each other.

7. Experiment with dissipative multi-pulse acousto-optical coupled states in a crystal with square-law nonlinearity and linear acoustic losses

To realize experimentally shaping the dissipative multi-pulse three-wave weakly coupled states by the continuous-wave optical pump in a two-mode medium with linear losses for a relatively slow non-optical wave the acoustic phonon mechanism of light scattering had been used. The schematic arrangement of the experimental set-up exploited is shown in figure 5 and consists of a continuous-wave laser, a crystalline acousto-optical cell with a pair of polarizers (whose combined

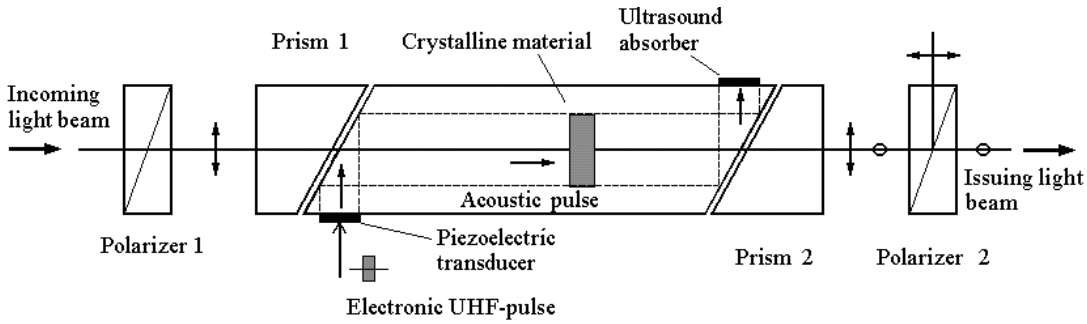

Figure 6. Scheme of the co-propagating collinear calcium molybdate acousto-optical cell providing the traveling-wave regime of interaction of the pumping light beam with the acoustic pulses.

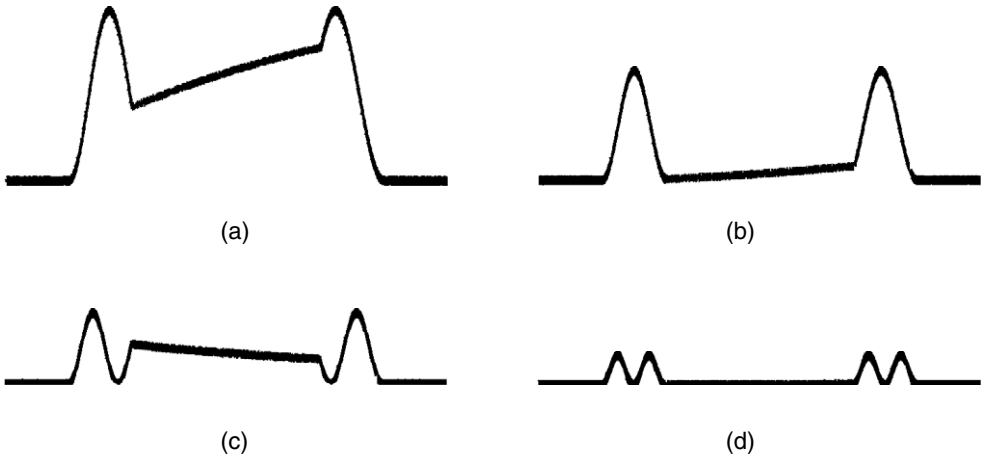

Figure 7. The digitized oscilloscope traces for the scattered light component intensity $|C_1|^2$ measured in a $CaMoO_4$ crystalline cell with $\alpha = 0.05\ \mathrm{cm}^{-1}$ at a carrier acoustic frequency of 61.3 MHz. Four stages of reshaping are followed at the same optical pump and acoustic wave intensities and temporal scales: (a) $\eta = 1.5\ \mathrm{cm}^{-1}$, the beginning stage of shaping a one-pulse coupled state; (b) $\eta = 2.4\ \mathrm{cm}^{-1}$, a one-pulse coupled state; (c) $\eta = 3.5\ \mathrm{cm}^{-1}$, an intermediate stage; and (d) $\eta = 6.0\ \mathrm{cm}^{-1}$, a two-pulse coupled state.

scheme is presented in detail separately in figure 6), a photodetector and a set of electronic equipment for generating and registering the corresponding electrical radio-wave (RW) signals. This scheme has some analogies with schemes for filtering optical signals [12], but allows operation in the pulsed regime. Initially, an electronic video pulse, determining a rectangular shape of the envelope, is provided from the pulse generator. Due to applying this video pulse to the ultra-high frequency (UHF) generator in the regime of an external modulation, an RW electronic UHF pulse can be obtained. Then, the shaped UHF pulse is applied to the electronic input of the collinear acousto-optical cell, see figure 6, and to the oscilloscope as the etalon signal, see figure 5.

A two-mode co-propagating collinear $CaMoO_4$ crystalline cell was characterized by a crystal length L of 44 mm along the [100] axis and an acoustic velocity v of $2.95 \times 10^5\ \mathrm{cm\ s}^{-1}$ for the shear elastic mode whose displacement vector is oriented along the [001] axis. The continuous-wave beam at a green light wavelength of 532 nm was used as an optical pump during the experiments. The first polarizer was precisely aligned in correspondence with the optical axes of a crystal in a cell. After the interaction with an acoustic pulse, already two orthogonally polarized light beams, the incident and signal ones, passed through a cell. The second polarizer gave us an opportunity to be aligned in correspondence with the polarization of the signal beam and to extract the output optical signal.

The dynamics of shaping and localizing the optical components of multi-pulse coupled states has been sequentially followed during our experiments. A few examples of the corresponding digitized oscilloscope traces are shown in figure 7. The maximal efficiency of shaping one-, two- and three-pulse optical components in the scattered light wave C_1 (shifted by the acoustic frequency from the pumping light wave C_0) was about 50% relative to the pumping light intensity with the excited acoustic power density of up to 0.5 $\mathrm{W\ mm}^{-2}$, which provided magnitudes of the parameter σ up to 2 cm^{-1}. The maximum frequency mismatch $\Delta f = \eta v/\pi$ was about 0.6 MHz, providing magnitudes of the phase mismatch η up to 6.32 cm^{-1}. The factor α of the linear elastic losses was about 0.05 cm^{-1} inherent in the chosen shear acoustic mode in a two-mode calcium molybdate crystalline acousto-optical cell at a carrier frequency of 61.3 MHz, which was determined by $\lambda = vf^{-1}|n_0 - n_e|$ [13]. The total length of a crystal is $L = 44$ mm, which provides a temporal aperture T of 15 μs. The duration of the rectangular acoustic pulse is taken to be $\tau_0 = 3.75\ \mu$s, which corresponds to a pulse spatial length l_0 of about 11 mm.

8. Discussion and conclusion

Let us discuss a set of obtained oscilloscope traces for the scattered light component intensity $|C_1|^2$ detected during the experiments with a $CaMoO_4$ crystalline cell. All these traces can be easily interpreted in terms of the above-mentioned three-stage picture, see section 5. The first stage is related to the process of localizing the scattered light when a rectangular acoustic pulse with a carrier frequency of 61.3 MHz is incoming through the input facet $x = 0$ of a cell. At this stage, the light, detected by a photodetector, reflects the dynamics of localizing the light wave $|C_1|^2$ whose degree of localization is determined by the value η of mismatch. In the two most impressive cases, see figures 7(b) and (d), the degrees of localizing the scattered light are close to total localization, so that practically one can observe a one-pulse or a two pulse dissipative coupled state, respectively. The second stage, connected with passing the localizing acoustic pulse along the cell, is characterized by a visible contribution of acoustic losses, which vary the output level of the scattered light for intermediate cases, see figures 7(a) and (c), or deform the localization inside coupled states. After passing through a cell, the loss-perturbed acoustic pulse is issued through the output facet $x = L$ of that cell. Leaving aside the effect of linear acoustic losses for a moment, one can say that the last stage demonstrates an almost mirror reflection of the first stage. In reality, however, the linear acoustic losses exist and give the corresponding contribution. In the particular case of total localization, the issuing acoustic pulse is destroying a multi-pulse coupled state, so that one can see this process in the oscilloscope traces as well, see figures 7(b) and (d). Consequently, the presented traces give us an opportunity to follow the dynamics of shaping and destroying the dissipative multi-pulse acousto-optical weakly coupled states in the collinear $CaMoO_4$ crystalline cell.

Thus, one can conclude that we have revealed and studied the dissipative multi-pulse three-wave weakly coupled states, appearing with collinear Bragg light scattering in a periodically modulated two-mode square-law nonlinear medium with linear losses for a slow non-optical wave. The localization conditions and spatio-temporal distributions of their optical components have been obtained in a new specific regime. Both quasi-stationary and non-stationary analytic models for describing the localization processes for multi-pulse three-wave coupled states have been elaborated. In so doing, the conditions of shaping background-free coupled acousto-optical states have been investigated and illustrated via the computer simulations. Finally, the results of our experiments with the dissipative multi-pulse three-wave weakly coupled acousto-optical states in a calcium molybdate crystalline cell have been presented and briefly discussed.

Acknowledgments

The work was financially supported by CONACyT, Mexico (project no. 61237) and the INAOE (Opto-Electronic project).

References

[1] Kivshar Y S and Agrawal G P 2003 *Optical Solitons: From Fibers to Photonic Crystals* (New York: Academic)
[2] Shcherbakov A S and Aguirre Lopez A 2003 Shaping the optical components of solitary three-wave weakly coupled states in a two-mode waveguide *Opt. Express* **11** 1643–9
[3] Shcherbakov A S and Aguirre Lopez A 2003 Binary encoded modulation of light based on collinear three-wave acousto-optical coupled states. *J. Opt. A: Pure Appl. Opt.* **5** 471–7
[4] Dodd K, Eilbeck J C, Gibbon J D and Morris H 1984 *Solitons and Nonlinear Wave Equations* (Orlando, FL: Academic)
[5] Ermakov V P 1880 Second-order differential equations; integrability conditions in the closed form *Universitetskie Izvestiya, Kiev.* (9) 1–25 (in Russian)
[6] Polyanin A D and Zaitsev V F 2003 *Handbook of Exact Solutions for Ordinary Differential Equations* 2nd edn (Boca Raton, FL: Chapman and Hall/CRC Press)
[7] Dixon R W 1967 Acoustic diffraction of light in anisotropic media *IEEE J. Quantum Electron.* **3** 85–93
[8] Balakshy V I, Parygin V N and Chirkov I E 1985 *Physical Principles of Acousto-Optics* (Moscow: Radio and Svyaz)
[9] Sirotin Yu I and Shaskolskaya M P 1982 *Fundamentals of Crystal Physics* (Moscow: Mir)
[10] Pinnow D A 1970 Guide lines for the selection of acousto-optic materials *IEEE J. Quantum Electron.* **6** 223–38
[11] Dmitriev V G, Guzalyan G G and Wikogosyan D N 1999 *Handbook of Nonlinear Optical Crystals* (New York: Springer)
[12] Yu F T S 2001 *Introduction to Information Optics* (San Diego, CA: Academic)
[13] Aksenov E T, Esepkina N A and Shcherbakov A S 1976 Acousto-optical filter with a $LiNbO_3$-crystal *Tech. Phys. Lett.* **2** 83–4